A Kinetic Model for Calcium Dynamics in RAW 264.7 Cells: 2. Knockdown Response and Long-Term Response

Mano Ram Maurya* and Shankar Subramaniam*†§
*Department of Bioengineering, †Department of Chemistry and Biochemistry, §Graduate Program in Bioinformatics, University of California, San Diego, La Jolla, California 92093

ABSTRACT This article addresses how quantitative models such as the one proposed in the companion article can be used to study cellular network perturbations such as knockdowns and pharmacological perturbations in a predictive manner. Using the kinetic model for cytosolic calcium dynamics in RAW 264.7 cells developed in the companion article, the calcium response to complement 5a (C5a) for the knockdown of seven proteins (C5a receptor; G-β-2; G-α,i-2,3; regulator of G-protein signaling-10; G-protein coupled receptor kinase-2; phospholipase C β-3; arrestin) is predicted and validated against the data from the Alliance for Cellular Signaling. The knockdown responses provide insights into how altered expressions of important proteins in disease states result in intermediate measurable phenotypes. Long-term response and long-term dose response have also been predicted, providing insights into how the receptor desensitization, internalization, and recycle result in tolerance. Sensitivity analysis of long-term response shows that the mechanisms and parameters in the receptor recycle path are important for long-term calcium dynamics.

INTRODUCTION

In the companion article (part 1), a kinetic model for calcium signaling in macrophage-like RAW 264.7 cells was developed for stimulation with the ligand complement 5a (C5a). Upon stimulation with C5a, cytosolic Ca^{2+} concentration ($[Ca^{2+}]_i$) increases, and this is attributed to ligand-induced release of calcium from the endoplasmic reticulum (ER) caused by increased activation and opening of the inositol 1,4,5-trisphosphate (IP_3) receptor (IP_3R) channels on the ER membrane. Activity of IP_3R channels is increased due to binding of IP_3 and Ca^{2+}. IP_3 is generated through hydrolysis of phosphatidylinositol 4,5-bisphosphate (PIP_2) into IP_3 and diacylglycerol (DAG) (1,2). Increased mobilization of calcium upon calcium binding to IP_3R is also referred to as calcium-induced calcium release (CICR) (3–5). Increased hydrolysis of PIP_2 is due to activated phospholipase C-β (PLCβ). The activation of the C5a receptor (C5aR) and the GTPase cycle of the G-protein G_i have been modeled in sufficient detail, including the desensitization, internalization, and recycling of the receptor (Fig. 1). The three-site model of IP_3 and Ca^{2+} binding to IP_3 receptor proposed by De Young and Keizer (6) and later simplified by Li and Rinzel (7) has been used to model calcium flux from the ER to the cytosol. The calcium released binds to various proteins such as calmodulin (CaM) to regulate downstream functions. Calcium is also pumped back to the ER by the sarco(endo)-plasmic reticulum calcium ATPase (SERCA) pump. Some calcium is expelled to the extracellular space through the Na^+/Ca^{2+} exchanger (NCX) and the plasma membrane calcium ATPase (PMCA) pump. Calcium exchange with the mitochondria also has been observed at elevated levels of $[Ca^{2+}]_i$ (8). Our model, despite being coarse grained and simple whenever possible, included the details of several mechanisms so that the knockdown (KD) of important proteins such as G-protein coupled receptor (GPCR) kinase (GRK) and GTPase-activating proteins (GAP) can be studied quantitatively (Fig. 1).

A quantitative model can be used to study the effect of structural/biochemical and parametric perturbations. Biochemical alterations such as under/overexpression of proteins have been implicated in many diseases. Examples relevant to the present model include decreased $G_{\alpha,i}$ levels in Alzheimer's disease (9) and increased blood pressure in regulator of G-protein signalling (RGS)$2^{-/-}$ mice (10,11). This article addresses how quantitative models such as the one proposed in the companion article can be used to predict the effect of cellular network perturbations such as KDs and pharmacological interventions, which can be validated experimentally.

Part 1 of this two-part article focused on the development of a kinetic model using the in vivo data exhibiting subpopulation variability from the Alliance for Cellular Signaling (AfCS) measurements (12). As discussed in part 1, most existing models have not explored the importance of the receptor desensitization, internalization, and recycling in long-term response. In this article we show that accurate modeling of the recovery processes is crucial for the understanding of the long-term behavior of calcium response and the downstream affected processes (13). The effect of KDs has also rarely been studied in a quantitative and kinetic context. This part (part 2) deals with the prediction and analyses of KD response and long-term response using the model developed

Submitted September 13, 2006, and accepted for publication February 27, 2007.

Address reprint requests to Shankar Subramaniam, Dept. of Bioengineering, University of California, San Diego, 9500 Gilman Drive, La Jolla, CA 92093-0412. Tel.: 858-822-0986; Fax: 858-822-5722; E-mail: shankar@ucsd.edu.

Editor: Ian Parker.

0006-3495/07/08/729/12 $2.00

doi: 10.1529/biophysj.106.097501

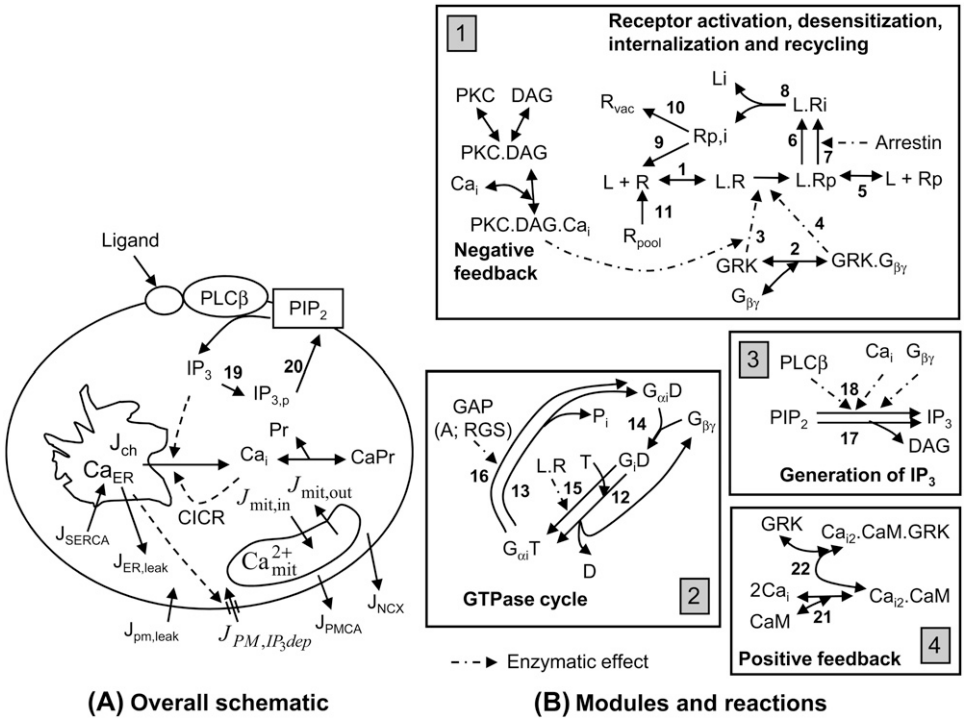

FIGURE 1 A simplified model for calcium dynamics. (*A*) Overall schematic model. The ligand C5a binds to its receptor C5aR on the plasma membrane (PM) activating G-protein G_i. The free subunit $G_{\beta\gamma}$ binds to and activates PLCβ, which hydrolyses PIP_2 into IP_3 and DAG. IP_3 binds to its receptor on the ER membrane, and the IP_3R channels open to release calcium into the cytosol (J_{ch} = calcium flux through the IP_3R channel, J_{PM,IP_3dep}= IP_3-dependent flux into the cytosol across the PM). Other calcium fluxes, e.g., with mitochondria and extracellular space, are also shown. (*B*) The mechanisms for the receptor module (*box 1*), GTPase cycle module (*box 2*), and IP_3 generation module (*box 3*), and the feedback effects (*boxes 1* and *4*). Abbreviations: $IP_{3,p}$, a lumped product of IP_3 phosphorylation; Ca_i, cytosolic Ca^{2+}; mit (subscript), mitochondria; L, ligand C5a; R, receptor C5aR; Arr, arrestin; P_i, phosphate.

in part 1. Fig. 1 (same as Fig. 1 in part 1) has been reproduced here for the purpose of clarity of the analyses presented. First the results of KD are presented as they have been validated qualitatively against the AfCS data. Sensitivity analysis of KD responses is also carried out. Then, the results on predicted long-term response, which serve as testable hypotheses, are presented. The KD response has revealed a multiplicity of features in calcium response. These include, with increasing KD, sharp initial decrease, increased basal level, increased rise time, and increased response. Further, our analysis of the long-term response provides an interesting finding, i.e., that the recycle path is important for calcium dynamics. This was not transparent in the study of short-term calcium response.

MATERIALS AND METHODS

To model the KD of a protein, using the values of the parameters (kinetic parameters, initial conditions, and buffered species concentrations) for the base case, the reduced value of the concerned parameter is computed as $x_{KD} = x\times(1 - \%knockdown/100)$ where x is the base value of the affected variable. Then any calculated parameters that could be dependent on the value of the variable being altered due to KD are computed and the new initial basal steady state is computed by allowing the system to evolve for ~1000 s and then solving the algebraic equations. The new basal state is computed whenever it is different from the initial basal state, e.g., when one or more parameters are changed. Besides this change, the simulations are carried out as described in Materials and Methods in the companion article.

KD response is predicted using the parameters for the master data set and with a 30 nM C5a stimulation for all KDs. Dynamic response upon ligand application under KD of seven different proteins, one at a time, has been simulated. In the AfCS experiments (14), these proteins are 1) the receptor C5aR (R), 2) G_β-2, 3) $G_{\alpha i}$-2,3 (a double KD), 4) the $G_{\alpha i}$ GAP, RGS10, 5) GPCR kinase, GRK2, 6) PLCβ-3, and 7) arrestin. In the model, these KDs are represented by reductions in the initial conditions of 1) C5aR (R), 2) $G_{\beta\gamma}$, and 3) $G_{\alpha i}D$; 4) the buffered level of the GAP, A; 5) GRK_{tot}; 6) $PLC\beta_{tot}$; and 7) the buffered level of arrestin. For the double KDs of $G_{\alpha i}$-2 and $G_{\alpha i}$-3, since both are isoforms of $G_{\alpha i}$ and we include only one isoform in our model for the sake of simplicity, this double KD is modeled by the (single) KD of IC:$G_{\alpha i}D$.

RESULTS

Prediction of knockdown response

Fig. 2 *A–F*, shows the temporal response of $[Ca^{2+}]_i$ and the KD response curve (peak height versus KD level) for the KD of six proteins. The KD levels simulated are 1%, 5%, 25%, 50%, 60%, 75%, 80%, 85%, and 90%. In Fig. 2, the response without KD (0% KD) is also included. The main results are presented below. For the KD of the seventh protein, arrestin, there is no noticeable change in $[Ca^{2+}]_i$ response in the short term (0–300 s). Hence, it is not shown in Fig. 2. By comparison with the in vivo data from AfCS (14), we have verified that the predicted KD response is qualitatively correct in terms of increase or decrease in the peak height for all KDs except for $G_{\alpha i}$, for which conflicting phenotypes have been observed in the AfCS experiments.

Knockdown of the receptor C5aR (R)

As shown in Fig. 2 *A*, with increasing levels of KD, peak height decreases (both *panels*) and the time to reach the peak increases (*left panel*). With decreasing R, in general,

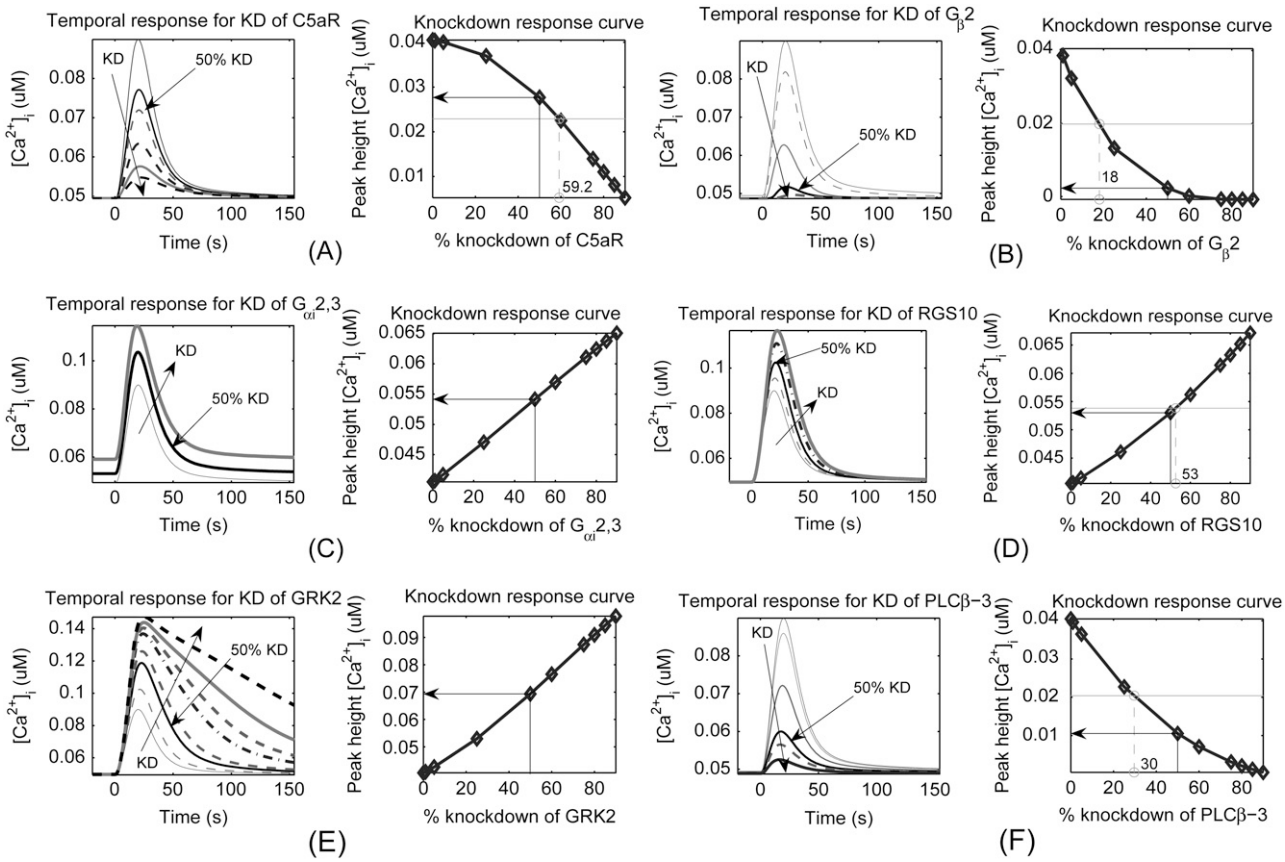

FIGURE 2 KD response predicted using the parameters for the master data set and 30 nM C5a for all KDs. For six KDs, the temporal response of $[Ca^{2+}]_i$ and the KD response curve (peak height versus KD level) are shown. (*A*) KD of C5aR. With an increasing level of KD, peak height decreases (both *panels*) and the time to reach peak increases (*left panel*). KD level required to reduce the peak height by 50% of the range of *y* axis is 59.2%. (*B*) KD of $G_{\beta\gamma}$. The response decreases with increasing KD similar to the KD of C5aR. However, initially, it decreases sharply compared to that at higher KD levels. Only 18% KD is required to reduce the peak height by 50% and at 50% KD, the peak height is reduced to 6%–8% level. (*C*) KD of $G_{\alpha i}$. With increasing KD, peak height increases in a proportional manner. Basal level also increases with increasing KD. (*D*) KD of the GAP RGS10. Most features of the temporal response and peak height are similar to that the KD of $G_{\alpha i}$ except that the basal response remains nearly unchanged. (*E*) KD of GRK. Although peak height increases with increasing KD more strongly compared to other KDs, the time to return to a specific percentage level, e.g., compared to the peak level for the chosen temporal curve, also increases (see text for explanation). (*F*) KD of PLCβ. The KD response is qualitatively similar to that of the KD of $G_{\beta\gamma}$. However, the response decreases less drastically. The KD level for 50% reduction in response is 30% compared to just 18% for the KD of $G_{\beta\gamma}$.

MAX([L.R]) also decreases. Thus, the activation level of the GTPase cycle decreases and lesser free $G_{\beta\gamma}$ is available. This leads to lesser activation of PLCβ and reduced hydrolysis of PIP_2 into IP_3, which results in a lowered flux of $[Ca^{2+}]$ from the ER to the cytosol and hence a lower peak is observed. The dynamic response for 50% KD is labeled with arrows in both the panels. The KD level required to reduce the peak height by 50% with respect to a scale normalized by the range of the *y* axis, i.e., 0% for the lowest peak (at 90% KD of C5aR) and 100% for the highest peak (no KD), is 59.2%. Since C5a and C5aR bind in 1:1 stoichiometry, with decreasing R_{tot}, there is little change in response up to 5% KD. Without KD, $R_{tot} \approx 0.04\ \mu M$. So, at 5% KD, $R_{tot} = 0.038\ \mu M$, which is still $\gg$30 nM (ligand strength). Thus, the dynamics of [L.R] remains almost the same. At 25% KD, some reduction in response is observed. At 50% KD, the response is reduced to the 65% level (peak height $\sim$0.028 μM). As R_{tot} is decreased the maximum peak height decreases and the half-maximal effect concentration (EC_{50}) for the dose response curve also decreases (not shown). It may be noted that the basal level does not change since, in our model, the receptor comes into play only upon stimulation by the ligand. In reality, due to the little basal activity of the receptor the basal level will decrease slightly, but it may be undetectable or may get nullified by the basal hydrolysis rate of PIP_2.

Knockdown of $G_{\beta\gamma}$

Decrease in total $G_{\beta\gamma}$ leads to reduced level of free $G_{\beta\gamma}$ (Fig. 2 *B*). This directly affects the rate of PIP_2 hydrolysis. Thus, the response decreases with increasing KD in a manner similar to the KD of C5aR. However, the decrease in response is higher at lower percentage KDs and plateaus at high KD. At very high KD, the differential decrease in response is almost zero. This can be explained by noting that

at very high KD, there is little free $G_{\beta\gamma}$ and the scenario is almost like the basal response. The initial sharp decrease is due to the fact that with increasing KD of the total $G_{\beta\gamma}$, the level of free $G_{\beta\gamma}$ decreases drastically. This is because the $G_{\beta\gamma,tot}$ and $G_{\alpha i,tot}$ are present in ~1:1 ratio in the absence of KD and that the α and $\beta\gamma$ subunits bind in a 1:1 ratio. Thus, when $G_{\beta\gamma,tot}$ drops below $G_{\alpha i,tot}$, $G_{\alpha i}D$ binds to almost all of it (see also the KD of $G_{\alpha i}$). GRK also competes for binding to $G_{\beta\gamma}$. Initially, with increasing KD, decrease in response is so drastic that only 18% KD is required to reduce the peak height by 50% and at 50% KD, the peak height is reduced to a 6%–8% level compared to the native cells. The basal level decreases slightly by the KD, but since basal activity of the GTPase cycle is already quite low and the intrinsic hydrolytic activity of PIP_2 is not affected, this decrease may not be detectable.

Knockdown of $G_{\alpha i}$ ($G_{\alpha i}D$)

Analogous to the explanation above, with increasing KD of $G_{\alpha i}$, more $G_{\beta\gamma}$ is free, nearly in a proportional manner since $G_{\beta\gamma,tot}$ and $G_{\alpha i,tot}$ are in an ~1:1 ratio in the native cells. Hence the peak height also increases accordingly (Fig. 2 *C*). One striking difference between the KD of $G_{\alpha i}$ and the KD of other proteins tested is that the basal level also increases with increasing KD. This is because with increased KD of $G_{\alpha i}$, the fraction of free $G_{\beta\gamma}$ in the basal state also increases. This amounts to having some G-protein activity without a stimulus.

Interpreting the results of this KD can be difficult and anomalous. We have been able to quantitatively capture this behavior by assuming that Ca^{2+} is able to enter the cytosol from the extracellular matrix (ECM) through leakage and an IP_3-dependent flux which serves as a feed-forward signal in regulating $[Ca^{2+}]_i$ (see the mathematical model in the Materials and Methods section in part 1). It has been suggested that the KD of $G_{\alpha i}$ may result in a decreased response since during stimulation chelator EDTA is used in the external medium. However, this is unlikely because after the KD, the cells grow for several generations and hence calcium must be present in the ECM during that phase. Necessary calcium will enter the cytosol and maintain a sufficiently high level of calcium in the ER in the basal state. It appears that the chelator is added a short time before the ligand addition. Although this results in the expulsion of some calcium to the ECM with $G_{\alpha i}$ KD since basal levels are high, the amount would not be large and hence $[Ca^{2+}]_{ER}$ at the time of ligand addition would not be too low though it would be lower compared to the value without KD of $G_{\alpha i}$. Notably, a lowered level of $[Ca^{2+}]_{ER}$ has been associated with Alzheimer's disease (15). Thus, upon stimulation, an increased peak should be observed, as is the case with the data set 3 used in the companion article. However, if the chelator is added long before the stimulation then $[Ca^{2+}]_{ER}$ can get very low. Hence, a reduced response would be observed. It can be noted that under such circumstances, the cells may expel all the calcium and die because the PMCA and NCX pumps are not blocked (16–18).

Knockdown of RGS10, a GAP (A) for $G_{\alpha i}$

Most features of the temporal response and peak height are similar to the KD of $G_{\alpha i}$ except that the basal response remains nearly unchanged (Fig. 2 *D*). With increasing KD, during stimulation lesser $G_{\alpha i}T$ is hydrolyzed into $G_{\alpha i}D$, so lesser $G_{\alpha i}D$ is present to bind to $G_{\beta\gamma}$ and, hence, more $G_{\beta\gamma}$ is in free active state. Further, the time to reach the peak increases with increasing KD. This is because after ligand addition, at any given time with the KD of RGS10 more free $G_{\beta\gamma}$ is available compared to the native cells. Higher $[G_{\beta\gamma}]$ results in increased activation of PLCβ, leading to increased production of $[IP_3]$. The resulting increase in channel flux, J_{ch}, leads to higher peak response. Also, KD of RGS10 means slower turning off of the GTPase cycle (19). Thus, a larger channel flux is observed for a longer time. The cumulative effect is the increased peak response and larger time required to attain that response.

Knockdown of GRK

The phenotype of GRK KD is different from others in two aspects: 1) the peak height increases with increasing KD more strongly compared to other KDs (Fig. 2 *E*); and 2) the time to return to a specific percentage level, e.g., compared to the peak response of the chosen temporal curve, also increases. For other KDs the fall time nearly remains unchanged (Fig. 2 *E*). This is because with lowered GRK the receptor and hence the GTPase cycle is active for longer times. In fact, with increasing KD, the flux through the SERCA pump becomes more and more responsible for the decrease phase. As opposed to this, for all other KD scenarios, the turning off of the receptor and the GTPase cycle modules themselves are equally responsible for attaining the peak and the subsequent decrease in $[Ca^{2+}]_i$. Due to delayed turning off of the receptor activity, the time to reach the peak is also increased. This feature is similar to the KD of RGS10 presented above. The KD response is nearly linear here, in a manner similar to the KD of $G_{\alpha i}$ and RGS10. At very large KD of GRK, there is little phosphorylation of the active receptor. Thus, the receptor is active for more than 100–200 s. Due to this prolonged activity, both the channel J_{ch} and J_{SERCA} saturate or, more precisely, level off due to their M-M or Hill kinetics dependence on $[IP_3]$ and/or $[Ca^{2+}]_i$. Hence, the difference of J_{ch} and J_{SERCA} is also nearly constant. This results in a linear decrease in response in the time domain (Fig. 2 *E*, *left panel*).

Knockdown of PLCβ

With increasing KD levels of PLCβ, the response of calcium decreases (Fig. 2 *F*). The KD response is qualitatively similar to that of the KD of $G_{\beta\gamma}$. However, the response decreases

less drastically. The KD level for 50% reduction in response is 30% compared to merely 18% for the KD of $G_{\beta\gamma}$. Similarly, at 50% KD, response is reduced to the 25% level compared to the 6%–8% level for 50% KD of $G_{\beta\gamma}$. The decrease in response was much sharper for the KD of $G_{\beta\gamma}$ since $G_{\beta\gamma}$ acted as a limiting reactant.

It is interesting to note that each of the KDs presented here has one or more special features, such as sharp initial decrease (Fig. 2 *B*), increased basal level (Fig. 2 *C*), increased rise time (Fig. 2 *D–E*), and increased response (Fig. 2, *C–E*). These features are summarized in Table 1. Further, all KDs that result in increased response are linear, whereas the rest exhibit nonlinear KD response curves. This is because the main focal point of increase in response is the increase in the release of calcium from ER. Due to the saturation effect, e.g., through the Michaelis-Menten parameter, K_M, once sufficiently high levels are reached, further increase in the flux is small despite the third-power dependence of the calcium flux through the IP_3R-channel, J_{ch}, on h and other M-M-like terms (7). On the other hand, with decreasing response, we move away from the saturation region into the more linear region of M-M kinetics, resulting in a sharper decrease in peak height due to the third-power dependence.

Since these results are based on the parameters for the master data set only, when comparing to experimental data from the KD cell lines, only qualitative comparison should be made because due to subpopulation variability, excessive differences in one or more of the capacity-like parameters such as $PLC\beta_{tot}$ may counterbalance the expected behavior. As an example, peak height for 50% KD in Fig. 2 *F* (based on data set 1) is lower than that for 83% KD in Fig. 3 *D* (*panel* 2) of part 1 that is based on data set 4. This can be explained by subpopulation variability. In particular, $PLC\beta_{tot,set\ 4}/PLC\beta_{tot,set\ 1}$ is 1.44 (optimized) in the absence of KD. Hence, in data set 4, even with higher KD of $PLC\beta$, a higher peak is observed.

Possible approach to quantitative validation of knockdown response

As indicated above, quantitative experimental validation will require controlling the subpopulation variability between the control cell line and the KD cell line. This may be achieved in two ways. The first is to perform cell cycle synchronization in both control and KD cell lines before harvesting the cells for ligand application. This can be achieved by arresting the cells in a specific phase using appropriate pharmacological inhibitors or through serum deprivation, which would arguably not interact with the KD of interest; see Davis et al. (20) and Chou and Langan (21) for a review. Cooper (22,23) has discussed potential drawbacks of a serum deprivation method. With cell cycle synchronization in place, the response for a chosen dose of C5a in two different control cell lines should be nearly the same, provided the number of cells is large in both batches; any difference can only be attributed to experimental errors. Then, we anticipate a good quantitative match between the predicted and experimental KD response. The second approach, which indirectly attempts to emulate cell cycle synchronization without experimentally enforcing it, is to prepare a very large batch of growing cells and then divide them into thousands of subpopulations. If one could locate two subpopulations with nearly identical molecular properties such as basal calcium levels, potentially they would be in synchronization. One subpopulation can be harvested for control study and the other for the KD study. We note that although the second approach would avoid the unwanted effects of pharmacological inhibitors, it may be less practical due to the very large batch size required and the difficulty in locating potentially synchronized batches.

Sensitivity analysis of knockdown response

Fig. 3 shows the alterations in the KD response when the parameter IC:[R] or R_{tot} is varied. The KD of R itself is not shown here. Panels 1–6 show the response surface for the KD of $PLC\beta$, arrestin, $G_{\beta\gamma}$, GRK, $G_{\alpha i}D$, and RGS10, respectively. The z axis is the peak height compared to the basal level for the base case. The response surfaces shown in panels 1 and 3 have three limiting regimes, only two in panel 2, and four limiting regimes in panels 4–6. In panel 1, the limiting regimes correspond to: a), low KD of $PLC\beta$ and low IC:[R]; b), low KD and high IC:[R]; and c), high KD and any value of IC:[R]. In panel 2, only two limiting regimes are

TABLE 1 The main features of the predicted KD responses of various proteins

	Features of KD response with increasing KD level			
Protein name	Peak height	Basal level	Rise time	Decay time constant
C5aR	decreases, concave	no change	increases (2–4 s)	increases (12 s)
G_β-2($G_{\beta\gamma}$)	decreases sharply, convex	small decrease (~1 nM)	*	*
$G_{\alpha i}$-2,3($G_{\alpha i}$)	increases, linear	increases (10 nM)	no change	increases (~4 s)
RGS10	increases, linear	no change	increases (2–4 s)	increases (~4 s)
GRK2	increases, linear	no change	increases (4–6 s)	increases (2 min)
$PLC\beta$-3	decreases, convex	small decrease (~1 nM)	decreases (3–5 s)	increases (7 s)

The rise time and decay time constant are assessed by normalizing and synchronizing the peaks for all KD levels. Rise time is taken as the time to reach the peak. The decay time constant is the time required for the normalized response (basal level = 0, peak = 1) to decrease from the peak level to 0.37 ($= e^{-1}$).
*It is difficult to assess the rise time and decay time constant since peak height is almost zero for 60% or higher KD levels.

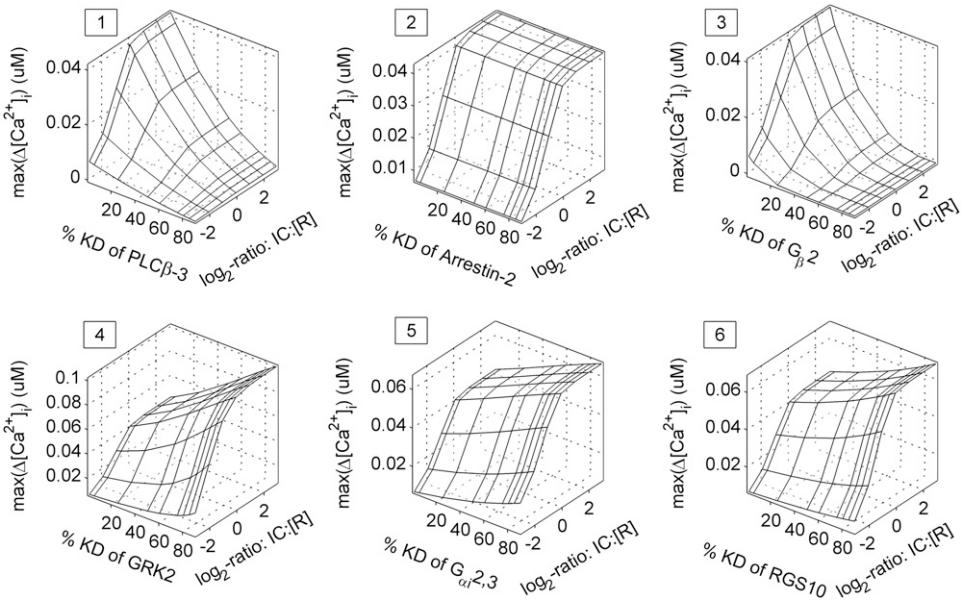

FIGURE 3 KD response of various proteins for variation in the parameter IC:[R], the total surface receptor. In each panel, the *x* axis is the percentage KD of the chosen protein, and the *y* axis, on $\log_2$ scale, is the perturbation ratio for IC:[R] compared to its base value. The *z* axis is the peak height. Panels *1–6* are for the sensitivity of the KD response of PLCβ, arrestin, $G_{\beta\gamma}$, GRK, $G_{\alpha i}$D, and RGS10, respectively.

observed since the KD of arrestin has no impact on the short-term response. The features of the response surface in panel 3 are similar to that in panel 1 because the rate of hydrolysis of PIP_2 is affected by both PLCβ_{tot} and $G_{\beta\gamma}$ in a similar manner (reaction 18). The response surfaces in panels 4–6 are more interesting, resulting in four limiting regimes since the KD of these proteins also results in increased response (Fig. 2, *C–E*).

Receptor desensitization, internalization, and recycling

Although receptor recovery has been studied in the context of G-protein signaling (24–26), it has been almost ignored in the context of calcium signaling except for the recent study by Lemon et al. (1). Hence, an in-depth analysis of receptor recovery is carried out here. As stated in Table S4 of part 1, the rate constant for receptor recycling (reaction 9), $k_{f,9}$, is set to 0.001/s. This value may be somewhat higher than reported in the literature (24), but it has little impact on the short-term response. The increased value is used to recover most of the receptors in ~1 h. Sample simulations with other values of $k_{f,9}$ have shown that qualitative features of the model do not change.

Long-term response and application of a second dose of C5a of equal strength

Fig. 4 *A* shows the fraction of free surface receptors over a period of 0–5000 s (~84 min) when 30 nM C5a is applied at t_{LA} (time of ligand addition) = 0 s. It takes ~30 min to recover 80% of the receptors and more than 90% of the receptor is recovered in 60 min. Since $k_{f,9}$ is the smallest of all the rate constants in the recycle path ($k_{f,6}$, $k_{f,7}$*[Arr], and $k_{f,8}$), it is the rate-limiting step. Once the fraction of surface receptors ($[R]/R_{tot}$) reaches its minimum of ~25%, the remaining response appears like a first-order process with a time constant of ~1250 s.

If a second dose is applied soon after the first dose, then due to fast desensitization of the receptors, a lower second

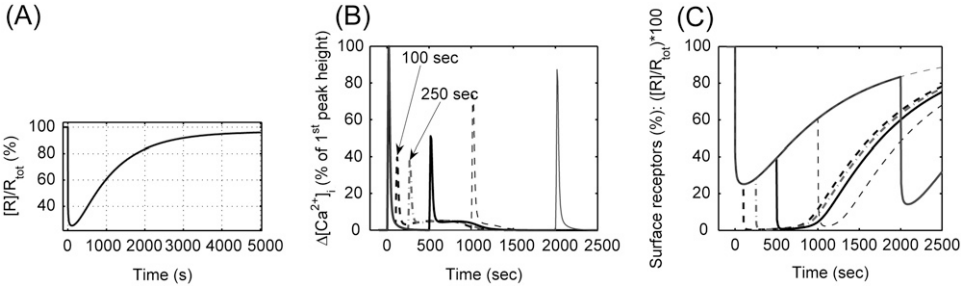

FIGURE 4 Prediction of long-term response using the parameters for data set 1 and 30 nM C5a dose. Recovery of the receptor in the log term and the effect of a second dose of 30 nM C5a is shown. (*A*) Dynamic response of the free surface receptors, represented as a percentage of total surface receptors. (*B*) Response with a second dose of 30 nM C5a. The first dose is applied at 0 s in each case. The second dose is applied at different times. $[Ca^{2+}]_i$ response is shown as change from the basal level as a percentage of the height of the first peak after $t_{LA} = 0$ s. With increasing t_{LA} for the second dose, height of the second peak increases since more receptors have been recovered when the second dose is applied. (*C*) Fraction of surface receptors corresponding to (*B*). The top curve (*thin dashed*) depicts the response if only one dose were to be applied. The other curves, which appear to separate from the top curve after the time of applying the second dose, depict the response after that time.

peak is obtained whereas if applied a sufficiently long time after the first dose, much of the response is recovered due to the internalization and the subsequent recycling of the receptor. Fig. 4, *B* and *C*, shows the response of $[Ca^{2+}]_i$ and [R] when one dose of 30 nM C5a is applied at 0 s (denoted $t_{LA,1}$); and in the same set of simulation, a second dose of 30 nM C5a is applied at different times ($t_{LA,2} = 100$, 250, 500, 1000, and 2000 s). Fig. 4 *B* shows normalized $[Ca^{2+}]_i$ response. In Fig. 4 *C*, the top curve (*thin dashed*) depicts the response if only one dose were to be applied. The other curves, which appear to separate from the top curve after $t = t_{LA,2}$, depict the response after $t_{LA,2}$. In general, with increasing $t_{LA,2}$, the height of the second peak of $[Ca^{2+}]_i$ increases since more receptors have been recovered when the second dose is applied. The second peak is a little higher for $t_{LA,2} = 100$ s compared to for $t_{LA,2} = 250$ s since $[Ca^{2+}]_i$ has not yet returned to basal level at 100 s, thus bringing in the effect of CICR. At later times, more and more receptor is recovered through reactions 6–9. Hence, a nearly complete response (~90%) is obtained for $t_{LA,2} = 2000$ s.

Another interesting observation in Fig. 4 *B* is that for the response due to the second dose at $t_{LA,2} = 100$, 200, 500, and 1000 s, a third peak of very low height is obtained. This is because for these cases, even after the second major peak, some ligand is left unused which binds to free surface receptors, if available. The third peak is only a minor peak because [R] drops to zero or is very small around the second peak. It is interesting that even with very small amounts of R, as long as some unused ligand is present, a response several times greater than $[R]/R_{tot}$ is observed for the third peak. Indeed, the receptor module exhibits interesting input response complexity.

Long-term dose response

We wanted to find if a single dose could result in more than one peak. It turns out that this is dose dependent because to get a second peak, both the receptor and ligand must be present. And to get the receptor recycled, the ligand must be separated (reaction 8). This separated internalized ligand is ubiquitinated and proteolyzed. Thus, in each cycle of the receptor recovery, an equal amount of ligand is degraded. Also, due to the affinity of the ligand for the receptor, only a small fraction of the ligand or the receptor (whichever is limiting) remains unbound. This suggests that to observe a second peak, the dose would have to be larger than R_{tot}. This is validated by simulation results.

Only one peak is obtained for C5a dose $\leq R_{tot} = 40$ nM, but two peaks (or one peak and one plateau) are obtained for C5a $>$ 40 nM. Fig. 5 *A* shows the temporal response of $[Ca^{2+}]_i$ (normalized) for increasing dose of C5a applied at $t_{LA} = 0$. In Fig. 5 *A*, the temporal responses for the doses resulting in a second peak or plateau are labeled. The *y* axis has been truncated at 20% to better display the second peak or plateau. At low doses up to C5a $\leq$ 40 nM, only a single

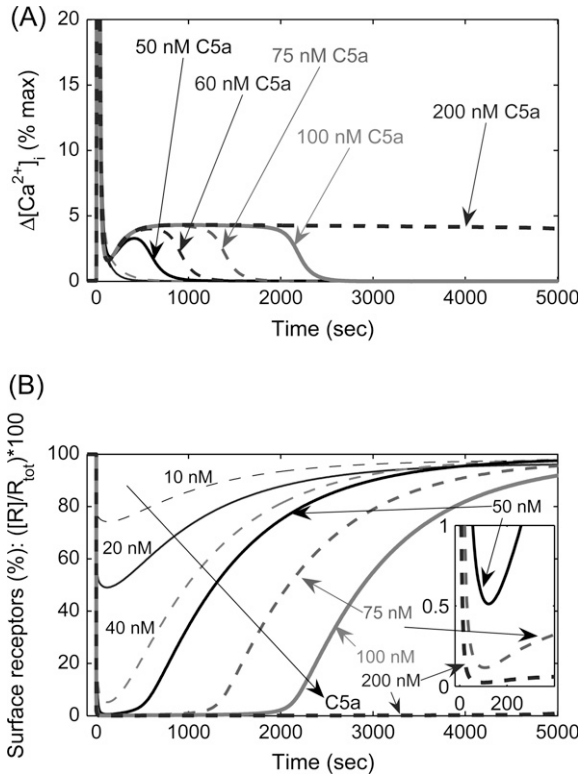

FIGURE 5 Long-term dose response. Increasing dose of C5a is applied at $t_{LA} = 0$ s and the system is simulated for 5000 s. The temporal responses for the doses resulting in a second peak or plateau are labeled. (*A*) Temporal response of $[Ca^{2+}]_i$ expressed as deviation from basal level as percentage of maximum peak height for the first peak across all doses. The *y* axis has been clipped at 20% to better see the second peak. No second peak is observed for C5a $\leq$ 40 nM. A clear second peak is obtained for C5a = 50 nM. As C5a is further increased, the height of the second peak remains unchanged, but it becomes a plateau. (*B*) Fraction of surface receptors with increasing dose. For C5a $\leq$ 40 nM, the minimum fraction does not drop below 5%, whereas for higher doses it drops to near zero, as shown in the inset (~0.5% up to 50 s for 50 nM and 0.02%–0.05% up to 1000 s for 200 nM).

peak is observed because by the time enough receptor is recycled, all the ligand is degraded. A clear second peak is obtained for C5a = 50 nM. As C5a is further increased beyond 60 nM, the height of the second peak remains the same, but its shape becomes more like a plateau. For C5a = 200 nM, the plateau remains for hours. Fig. 5 *B* shows the fraction of surface receptors with increasing dose. For C5a $\leq$ 40 nM, the minimum fraction does not drop below 5%, whereas for higher doses it drops to near zero as shown in the inset. The minimum fraction drops to ~0.5% up to 50 s for 50 nM C5a and to 0.02%–0.05% up to 1000 s for 200 nM C5a. With increasing doses, $[R]/R_{tot}$ remains close to zero for a longer time. In fact, the qualitative shapes of $\Delta[Ca^{2+}]_i$ and $[R]/R_{tot}$ are inversely correlated. As $[R]/R_{tot}$ starts to increase substantially $\Delta[Ca^{2+}]_i$ begins to drop. This is because as long as some ligand is present, it has a tendency to bind to the receptor and hence keep $[R]/R_{tot}$ very low. Most of it is either in the internalized form or is bound to the ligand and hence a finite $[Ca^{2+}]_i$ is observed. Once all the ligand is degraded,

more and more receptors remain free after recycling. Hence, $[R]/R_{tot}$ starts to increase and [L.R] drops quickly, resulting in decreasing $[Ca^{2+}]_i$. In short, the occurrence of the second peak at C5a $>$ 40 nM is directly correlated with R_{tot} ~40 nM with implications for inferring the total pool of surface receptors.

It is interesting that a third peak cannot be obtained even for very high doses. This is because to observe a third peak, [C5a] must drop to zero and once this happens [C5a] cannot increase again since it is only the receptor that is recovered through recycling after internalization and not the ligand.

Beyond 60 nM C5a, it is not the height but the duration of the second peak that increases. It is also interesting to note that with increasing doses beyond 60 nM C5a, it is not the height of the second peak that increases. Instead, the response stays at this level for a longer time. The underlying reason is that during this time frame, since ligand is present in excess amounts and the receptor is the limiting species, for all practical purposes, a lower-order system is established in which a pseudo-steady state is attained and the ligand is degraded at a nearly constant rate and that [L.R] remains constant. In terms of the dynamics in the downstream modules, a pseudo-steady state is established since the channel flux is maintained over the plateau. Such responses can be utilized for optimal design of drug dosage and release rate for maximum efficacy in pharmacodynamic studies. For example, the data in Fig. 5 *A* suggest that the overall large dose (e.g., >100 nM) can be administered in a ramp-wise fashion up to 200 s to achieve almost uniform response without exceeding a predefined first peak response.

Quantitative characterization of receptor desensitization: dose response with a second dose applied at a fixed time

In the results discussed above, in one case two doses of 30 nM C5a were applied at different times and in the other case, long-term response for a single dose with increasing strength was predicted. The latter can be used to construct both the receptor activation and receptor desensitization curves by recording the peak of [L.R] and the minimum point of [R] after applying the ligand. However, these are rarely measured directly. Hence, peak $\Delta[Ca^{2+}]_i$ measurements are used to construct the activation and desensitization curves (1). The activation curve is essentially a normalized dose response curve. The desensitization curve is constructed by applying a second dose at a fixed time later either of strength equivalent to EC_{50} levels (1,27) or of the same strength as the first dose. We have carried out both. The time of applying the second dose ($t_{LA,2}$) is chosen so that the source chemicals, such as PIP_2 and $[Ca^{2+}]_{ER}$, in the downstream part have returned to their basal levels. Also, the receptor should not have been recycled significantly. In our case, we have chosen $t_{LA,2}$ = 250 s ($t_{LA,1}$ = 0 s). The essential idea behind applying the second dose of the same strength is that we want to see the response if the same external conditions are created repeatedly. The dose levels are C5a = [1, 2, 5, 10, 20, 30, 40, 50, 60, 75, 100, 200, 400, 800] nM.

Second dose of equal strength

Fig. 6 *A* shows the dynamic response for three different ligand strengths, viz. 10, 20, and 40 nM C5a. The maximum response used for normalization is the same as the height of the first peak for C5a = 800 nM. For clarity, the dynamic responses for other doses are not shown in Fig. 6 *A*. For each curve, the ratio of the second peak height ($\Delta[Ca^{2+}]_i$) to the first peak height is computed. This ratio is a measure of desensitization.

Second dose of EC_{50} strength

Fig. 6 *B* shows the temporal responses for the three cases when the second dose is of $R_{tot}/2$ strength, which is closely related to the EC_{50} value for the ligand. However, this time,

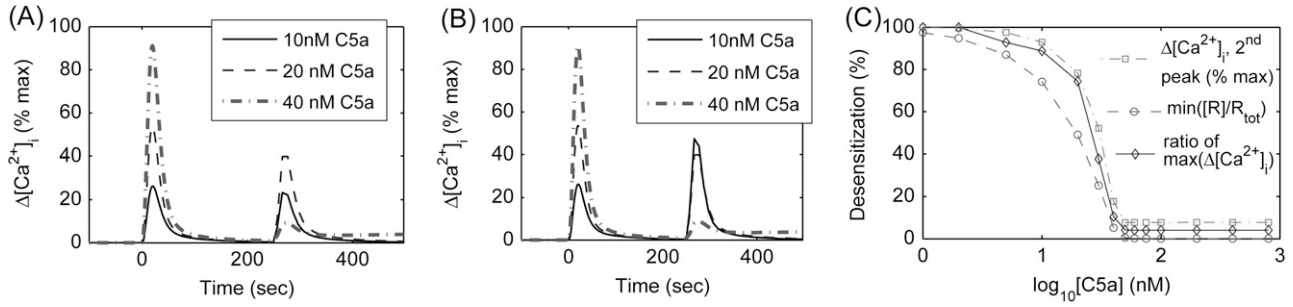

FIGURE 6 The desensitization of the receptor at varying doses. Two doses are applied at $t_{LA,1} = 0$ s and $t_{LA,2} = 250$ s, respectively. (*A*) Temporal responses, normalized with respect to the largest first peak, are shown for the first dose = 10, 20, and 40 nM. The second dose is the same as the first dose. From each curve, the ratio of the height of the second peak to that of the first peak is computed for use in *C*. (*B*) Normalized temporal responses with the second dose of half-maximal EC_{50} strength (1,27) are shown. Here, the height of the second peak expressed as a fraction of the maximum height of the second peak is used for *C*. (*C*) The desensitization curves computed using data from (*A*) (◇), (*B*) (□), and the minimum value of $[R]/R_{tot}$ between $0 < t < 250$ s (*dash dot* with *circle marks*). The results from both (*A*) and (*B*) are quite similar even quantitatively. Half-maximal inhibitory concentration (IC_{50}) value for the curve from data in (*B*) is ~31 nM. At very high doses, (*A*) and (*B*) saturate to nonzero values since even a tiny amount of the receptor (due to recycling) is able to result in a proportionally larger response due to sufficient ligand strength.

instead of computing the ratio of the two peaks for each curve, the height of the second peak is normalized by the maximum of the second peak height. These data also characterize the desensitization (1,27).

Desensitization curves using calcium response

The two sets of data on desensitization are plotted in Fig. 6 *C* (data from Fig. 6 *A*, ◇; data from Fig. 6 *B*, □). For both the curves, at low doses the ratio is close to 100%, starts to decrease as the dose strength increases, and saturates to a very low value. The saturated response is not exactly zero since at high ligand strength as soon as a tiny amount of receptor is recycled the unused ligand binds to it to elicit some response. At very high doses, the saturation level of the data from Fig. 6 *A* is about half compared to the data from Fig. 6 *B*. This is because, in Fig. 6 *B*, the maximum peak height of the second peak is the same as the height of the first peak at EC_{50} strength, which is clearly half of the maximum height of the first peak in Fig. 6 *A*. Apart from this, both desensitization curves are very close. It is no surprise that Garrad et al. (27) used the second dose of EC_{50} strength in their experiments. The half-maximal inhibitory concentration (IC_{50}) value for the curve from data in Fig. 6 *B* is ~31 nM, which is higher from the EC_{50} value of 18 nM for the dose response curve (Fig. 6 *F* in the companion article). The qualitative shape of the desensitization curve matches the predictions of Lemon et al. (1) and experimental observations of Garrad et al. (27).

Desensitization curve using the receptor response

For completeness, in Fig. 6 *C*, we have also plotted $[R]_{min}/R_{tot}$ (computed between $0 < t < 250$ s) versus dose strength from the simulation data for Fig. 6 *A*. This plot lies below the other two desensitization curves because the fractional value of $[R]_{min}/R_{tot}$ is always smaller than the corresponding $[Ca^{2+}]_i$ response. This is partly due to CICR and partly due to the more than additive effect of the tiny amounts of the receptor. To understand the difference at lower doses, consider C5a = 10 nM as the first dose in Fig. 6 *B*. At the time the second dose is applied, [R] ~30 nM. The second dose is C5a = 20 nM. With $[R] = R_{tot} = 40$ nM, this had resulted in 50% of maximum of first peak height which is ~100% of the maximum of the second peak height. With 30 nM [R], the response will be somewhat lower. Fig. 6 *C* shows this to be ~90%. Similarly, with 20 nM C5a as the first dose, ~75% (normalized) response is achieved for the second peak, which is the right value for the 20 nM [R] and 20 nM C5a combination. Thus, quantitatively, all three desensitization curves support each other.

Possible approach to quantitative validation

Unlike the KD studies, for the above long-term response, all the experiments of Ca^{2+} measurement could be conducted on the same cell line within a time frame of 24 h. The time for full recovery of the receptor at a dose up to 100 nM is ~2 h. The dose used for the data shown in Fig. 4 is 30 nM. The maximum dose required for obtaining the data used in Figs. 5 and 6 is 200 nM. So, a gap of ~2.5 h between applying the dose corresponding to a new experiment (a particular curve in Fig. 4 *C*, Fig. 5, *A* and *B*, or Fig. 6, *A* and *B*) is adequate. Hence, 24 h are enough to generate data for validating the results shown in Figs. 4–6, one at a time or ~72 h to generate data for all three figures. It is assumed that the same cell line is used from which the data set 1 used for parameter constraining was generated because all predictions are based on the corresponding parameters. In fact, this is an interesting idea since, a fraction of the resulting experimental data can actually be used for parameter constraining.

Sensitivity analysis of long-term response

Long-term response is affected by both the parameters that affect the short-term response and the parameters related to the reactions involved in the receptor internalization ($k_{f,6}$, [Arr], and $k_{f,7}$), ligand separation ($k_{f,8}$), and the recycling of the receptor ($k_{f,9}$). Since all these reactions in the recycle path are in series and are of first order, the associated time constants could be potentially added and, hence, perturbation of any of these parameters has a similar effect. Fig. 7 shows the temporal response as a surface for perturbation in the parameter $k_{f,9}$ when two doses of 30 nM C5a are applied at 0 s ($t_{LA,1}$) and at 500 s ($t_{LA,2}$). The *z* axis is the deviation from the basal level expressed as a percentage of the height of the first peak. The short-term response and, hence, the height of

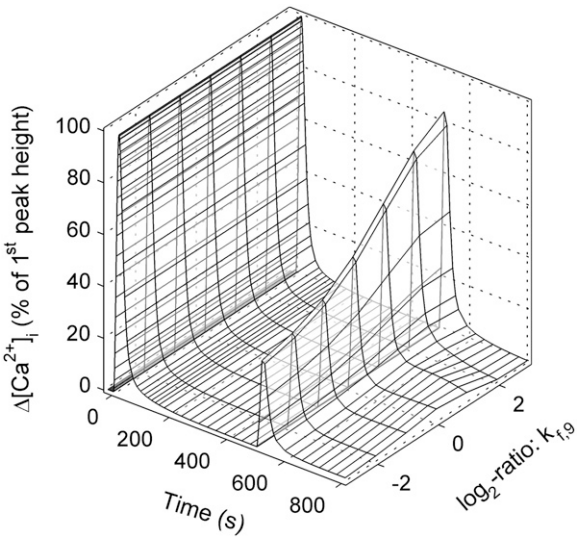

FIGURE 7 Long-term response with a second dose under perturbation in the parameter $k_{f,9}$. The *x* axis is the time, and the *y* axis is the $\log_2$ of the perturbation factor. First dose of 30 nM C5a is applied at 0 s. The second dose of 30 nM C5a is applied at 500 s. With increasing value of $k_{f,9}$, the height of the first peak remains unchanged but that of the second peak increases.

the first peak does not change due to perturbation in $k_{f,9}$. However, with increasing $k_{f,9}$, the receptor gets recycled faster, i.e., more surface receptors are available by the time $t = t_{LA,2} = 500$ s and, hence, the height of the second peak increases. Other parameters such as $k_{f,6}$, $k_{f,7}$, [Arr], and $k_{f,8}$ show a similar effect (not shown).

DISCUSSION

Using the model developed in part 1, the response of the system has been predicted for the KD of several proteins in the calcium network. Qualitative comparison with in vivo data on the KD response has helped validate our model. To correctly model the KDs resulting in changes in the basal levels, e.g., KD of $G_{\alpha,i}$, interaction with the ECM is critical. The recent evidence about IP_3R channels on the PM further provides strength to this effect (28). Our model included the mechanisms of receptor desensitization, internalization, and recycling, which are critical for accurate prediction of long-term response as revealed by single-parameter perturbation analysis of long-term response.

Knockdown response

KD response plays the same role in quantitative modeling of a biochemical system as knockout in network structure (qualitative) modeling (29). KD response can serve to characterize the efficacy of the RNA interference (RNAi)-based drugs (30). The KD response of most key players in the network shown in Fig. 1 has been carried out and has been qualitatively validated against the AfCS data. The KD response has revealed the multiplicity of features in calcium response (Table 1).

C5aR

C5a has been implicated in many disorders such as systemic inflammatory response syndrome during infection by Septicemia (31), which can result in septic shock. Our results show reduced G-protein activity and $[Ca^{2+}]_i$ response upon KD of C5aR (Fig. 2 *A*). These effects reduce the expression of inflammatory cytokines and the release of histamine.

G_{β}−2

The KD of $G_{\beta\gamma}$ results in a sharp reduction in calcium levels at low KDs (Fig. 2 *B*). $G_{\beta\gamma}$ has been termed one of the hot spots of signaling (32). It interacts with many pathways and proteins. Different binding sites on $G_{\beta\gamma}$, e.g., for G_{α}, phospholipases, and GRK, may be selectively targeted by small molecules for therapeutic applications (33).

$G_{\alpha i}$−2,3

KD of $G_{\alpha i}$ results in increased peak height and basal level of $[Ca^{2+}]_i$ response (Fig. 2 *C*). Decreased $G_{\alpha,i}$ levels have been reported in Alzheimer's disease (9). Interestingly, lowered $[Ca^{2+}]_{ER}$ has also been reported in Alzheimer's disease (15), and our KD modeling study has shown that KD of $G_{\alpha,i}$ results in decreased basal $[Ca^{2+}]_{ER}$.

RGS10

KD of RGS10 results in increased peak height of $[Ca^{2+}]_i$ response linearly (Fig. 2 *D*). The AfCS has carried out KDs on RGS2, RGS3, RGS10, and RGS16 in RAW 264.7 cells (14). Similar to the results of KD of RGS10, KD of RGS2 in hypertensive patients increases calcium mobilization induced by angiotensin II (34).

Knockdown of GRK2

KD of GRK results in increased and prolonged mobilization of calcium (Fig. 2 *E*) since the receptor remains active for a longer time. Thus, GRK regulates G-protein activity strongly. In a recent study, increased expression of GRK2 in human heart failure resulted in reduced β-adrenergic receptor-mediated G-protein signaling (35).

Knockdown of PLCβ-3

Similar to $G_{\beta\gamma}$, KD of PLCβ results in a sharp decrease in $[Ca^{2+}]_i$ (Fig. 2 *F*). RAW 264.7 cells express three isoforms, PLCβ-2–4 (14). Consistent with the supralinear gain, it is suggested that IP_3 production may be more efficiently regulated by altering the amount of PLCβ-1–4 than by altering the level of G-proteins ($G_{\alpha,q/11}$) (36).

Among all the KDs discussed above, except for the GPCR, all other proteins are inside the cell. Hence, their KD effect can be achieved only through RNAi, in most cases. However, since the receptor is at the plasma membrane, its KD effect can be achieved by its pharmacological inhibition.

Receptor desensitization, internalization, and recycling

We have extensively analyzed the receptor recovery part of the system. We have shown that although receptor recycling is not important for the quantitative modeling of the short-term response, its accurate modeling is critical for predicting the long-term response. An interesting application of characterizing the receptor recycle system could be in formulating optimal doses of agonists and antagonists to avoid excessive desensitization of the receptor (37). Another potential application is in understanding drug addiction and tolerance or loss of sensitivity (38). We have demonstrated that if a second dose is applied soon after the first dose, to achieve a certain level of subsaturated response, a higher dose is needed. In the simplest form, this is the basis of tolerance. Long-term dose response shows that when the dose becomes higher than the total pool of receptors, the response becomes bimodal instead of having just one peak.

The duration of the second peak but not the peak height increases as the dose strength is increased, becoming flat and thus taking the system into a pseudo-steady state at extremely high doses.

Comparison with previous models and experimental results

Receptor desensitization

As stated in the Results (Fig. 6, *B* and *C*), our receptor desensitization results are in agreement qualitatively with those for uridine triphosphate (UTP) with P_2Y_2 receptors presented by Lemon et al. (1) and Garrad et al. (27). An excellent semiquantitative agreement is also observed. For example, the ratio of the half-maximal inhibitory concentration (IC_{50}) value for the desensitization curve in Fig. 6 *B* ($\sim$31 nM) to the EC_{50} value for dose response curve (18 nM) 1.72 is in excellent agreement with those obtained by Lemon et al. (1) for UTP with P_2Y_2 receptors: EC_{50} for dose response = 250 nM, IC_{50} for desensitization curve = 430 nM, ratio = 1.72 (Fig. 7 *A* of Lemon et al. (1)).

Dose response of receptor internalization

Quantitative characterization of GPCR internalization is necessary for therapeutic applications of GPCR agonists (39). Fig. 4 shows the temporal response of calcium and surface receptors for different doses. The data from the same set of simulations are used to construct the dose response for receptor internalization. Fig. 8 shows the dose response curve for the internalized ligand-bound receptors (L.Ri). The dose response of L.Ri is consistent with the experimental observations of Conway et al. (40) for the ligand parathyroid hormone in HEK-293 cells. The EC_{50} value is 21 nM, which is slightly above the EC_{50} value of 18 nM for calcium response. A similar result is experimentally obtained by Conway et al., where the EC_{50} for internalization (35 nM, Fig. 6 *A* of Conway et al.) is somewhat higher than the EC_{50} value for cAMP production (Fig. 1 of Conway et al.). These results also qualitatively match with those for β(2)-adrenergic receptor in HEK-293 cells and CHO-K1 cells (Haasen et al. (41)).

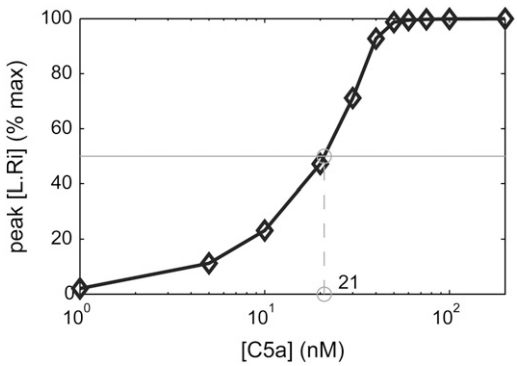

FIGURE 8 Dose response of internalized ligand-bound receptors (L.Ri) with increasing C5a. The *y* axis shows the normalized peak height. The sigmoid shape matches well with the experimental results of Conway et al. (40). The half-maximal EC_{50} is 21 nM.

Experimental construction of receptor desensitization or internalization requires experiments at several doses. Although experiments have to be carried out for novel (previously uncharacterized) GPCRs and their agonists, the total time and cost of experiments can be reduced through computational predictions made by a model that is based on experimental data for the chosen agonist-receptor system at several but at 2–3 times fewer doses. This philosophy of context-specific modeling holds promise for high throughput screening of GPCRs (39).

Limitations

Even though the model proposed included details of the GTPase cycle of G-protein G_i, other G-protein systems were not included due to the linear increase in the number of parameters to be estimated with the inclusion of additional experimental data. Though the qualitative response is not expected to change drastically if one were to include other GTPase cycles and the details of the PLCβ activation, quantitative differences are inevitable. Also, the level of detail is tailored toward predicting calcium response, and not the internal dynamics of individual modules. Hence, the lumped models of the modules may not be used for such purposes. Due to the existence of multiple parameter values with good fit to data, more emphasis should be on the qualitative interpretation of the results and the predictions. The same conclusion is arrived at due to the subcellular variability in the response. Similarly, some of the downstream processes, such as activation of Ca^{2+}/CaM-dependent kinases and other components which could feed back into the upstream parts of the network, are not included.

We acknowledge the Macrophage Biology Laboratory of the Alliance for Cellular Signaling (University of California, San Francisco) for the experimental data. We are grateful to the two anonymous reviewers for their insightful comments and suggestions.

This research was supported by the National Institutes of Health Collaborative Grants U54 GM62114 (Alliance for Cellular Signaling, S.S.) and U54 GM69338-04 (LIPID Metabolites and Pathways Strategy, S.S.), National Institutes of Health grant R01-GM068959 (S.S.), and a grant from the Hilblom foundation (S.S.).

REFERENCES

1. Lemon, G., W. G. Gibson, and M. R. Bennett. 2003. Metabotropic receptor activation, desensitization and sequestration-I: modelling calcium and inositol 1,4,5-trisphosphate dynamics following receptor activation. *J. Theor. Biol.* 223:93–111.
2. Mishra, J., and U. S. Bhalla. 2002. Simulations of inositol phosphate metabolism and its interaction with InsP(3)-mediated calcium release. *Biophys. J.* 83:1298–1316.

3. Berridge, M. J. 1990. Calcium oscillations. *J. Biol. Chem.* 265:9583–9586.
4. Berridge, M. J. 1992. Inositol trisphosphate and calcium oscillations. *Adv. Second Messenger Phosphoprotein Res.* 26:211–223.
5. Meyer, T., and L. Stryer. 1988. Molecular model for receptor-stimulated calcium spiking. *Proc. Natl. Acad. Sci. USA.* 85:5051–5055.
6. De Young, G. W., and J. Keizer. 1992. A single-pool inositol 1,4,5-trisphosphate-receptor-based model for agonist-stimulated oscillations in Ca^{2+} concentration. *Proc. Natl. Acad. Sci. USA.* 89:9895–9899.
7. Li, Y. X., and J. Rinzel. 1994. Equations for InsP3 receptor-mediated [Ca2+]i oscillations derived from a detailed kinetic model: a Hodgkin-Huxley like formalism. *J. Theor. Biol.* 166:461–473.
8. Marhl, M., T. Haberichter, M. Brumen, and R. Heinrich. 2000. Complex calcium oscillations and the role of mitochondria and cytosolic proteins. *Biosystems.* 57:75–86.
9. Young, R. A., K. Talbot, Z. Y. Gao, J. Q. Trojanowski, and B. A. Wolf. 1999. Phospholipase pathway in Alzheimer's disease brains: decrease in Galphai in dorsolateral prefrontal cortex. *Brain Res. Mol. Brain Res.* 66:188–190.
10. Gross, V., J. Tank, M. Obst, R. Plehm, K. J. Blumer, A. Diedrich, J. Jordan, and F. C. Luft. 2005. Autonomic nervous system and blood pressure regulation in RGS2-deficient mice. *Am. J. Physiol. Regul. Integr. Comp. Physiol.* 288:R1134–R1142.
11. Sun, X., K. M. Kaltenbronn, T. H. Steinberg, and K. J. Blumer. 2005. RGS2 is a mediator of nitric oxide action on blood pressure and vasoconstrictor signaling. *Mol. Pharmacol.* 67:631–639.
12. The Alliance for Cellular Signaling (AfCS). http://www.signaling-gateway.org/. Accessed August 16, 2006.
13. Christophe, T., M. J. Rabiet, M. Tardif, M. D. Milcent, and F. Boulay. 2000. Human complement 5a (C5a) anaphylatoxin receptor (CD88) phosphorylation sites and their specific role in receptor phosphorylation and attenuation of G protein-mediated responses. Desensitization of C5a receptor controls superoxide production but not receptor sequestration in HL-60 cells. *J. Biol. Chem.* 275:1656–1664.
14. The AfCS FXM signaling map. http://www.signaling-gateway.org/data/fxm/query?type=map. Accessed August 16, 2006.
15. Zatti, G., A. Burgo, M. Giacomello, L. Barbiero, R. Ghidoni, G. Sinigaglia, C. Florean, S. Bagnoli, G. Binetti, S. Sorbi, P. Pizzo, and C. Fasolato. 2006. Presenilin mutations linked to familial Alzheimer's disease reduce endoplasmic reticulum and Golgi apparatus calcium levels. *Cell Calcium.* 39:539–550.
16. Aneiros, E., S. Philipp, A. Lis, M. Freichel, and A. Cavalie. 2005. Modulation of Ca^{2+} signaling by Na^{+}/Ca^{2+} exchangers in mast cells. *J. Immunol.* 174:119–130.
17. Machaty, Z., J. J. Ramsoondar, A. J. Bonk, R. S. Prather, and K. R. Bondioli. 2002. Na^{+}/Ca^{2+} exchanger in porcine oocytes. *Biol. Reprod.* 67:1133–1139.
18. Reeves, J. P., and M. Condrescu. 2003. Allosteric activation of sodium-calcium exchange activity by calcium: persistence at low calcium concentrations. *J. Gen. Physiol.* 122:621–639.
19. Bornheimer, S. J., M. R. Maurya, M. G. Farquhar, and S. Subramaniam. 2004. Computational modeling reveals how interplay between components of a GTPase-cycle module regulates signal transduction. *Proc. Natl. Acad. Sci. USA.* 101:15899–15904.
20. Davis, P. K., A. Ho, and S. F. Dowdy. 2001. Biological methods for cell-cycle synchronization of mammalian cells. Biotechniques. 30:1322–6, 1328, 1330–1331.
21. Chou, R. C., and T. J. Langan. 2003. In vitro synchronization of mammalian astrocytic cultures by serum deprivation. *Brain Res. Brain Res. Protoc.* 11:162–167.
22. Cooper, S. 2002. Minimally disturbed, multicycle, and reproducible synchrony using a eukaryotic ''baby machine''. *Bioessays.* 24:499–501.
23. Cooper, S. 2005. Reanalysis of the protocol for in vitro synchronization of mammalian astrocytic cultures by serum deprivation. *Brain Res. Brain Res. Protoc.* 15:115–118.
24. Hoffman, J. F., J. J. Linderman, and G. M. Omann. 1996. Receptor up-regulation, internalization, and interconverting receptor states. Critical components of a quantitative description of *N*-formyl peptide-receptor dynamics in the neutrophil. *J. Biol. Chem.* 271:18394–18404.
25. Riccobene, T. A., G. M. Omann, and J. J. Linderman. 1999. Modeling activation and desensitization of G-protein coupled receptors provides insight into ligand efficacy. *J. Theor. Biol.* 200:207–222.
26. Woolf, P. J., and J. J. Linderman. 2003. Untangling ligand induced activation and desensitization of G-protein-coupled receptors. *Biophys. J.* 84:3–13.
27. Garrad, R. C., M. A. Otero, L. Erb, P. M. Theiss, L. L. Clarke, F. A. Gonzalez, J. T. Turner, and G. A. Weisman. 1998. Structural basis of agonist-induced desensitization and sequestration of the P2Y2 nucleotide receptor. Consequences of truncation of the C terminus. *J. Biol. Chem.* 273:29437–29444.
28. Vig, M., C. Peinelt, A. Beck, D. L. Koomoa, D. Rabah, M. Koblan-Huberson, S. Kraft, H. Turner, A. Fleig, R. Penner, and J. P. Kinet. 2006. CRACM1 is a plasma membrane protein essential for store-operated Ca^{2+} entry. *Science.* 312:1220–1223.
29. Janes, K. A., J. G. Albeck, S. Gaudet, P. K. Sorger, D. A. Lauffenburger, and M. B. Yaffe. 2005. A systems model of signaling identifies a molecular basis set for cytokine-induced apoptosis. *Science.* 310:1646–1653.
30. Clayton, J. 2004. RNA interference: the silent treatment. *Nature.* 431: 599–605.
31. Wikipedia. 2006. Systemic Inflammatory Response Syndrome. http://en.wikipedia.org/wiki/SIRS. Accessed August 2, 2006.
32. Tesmer, J. J. 2006. Pharmacology. Hitting the hot spots of cell signaling cascades. *Science.* 312:377–378.
33. Bonacci, T. M., J. L. Mathews, C. Yuan, D. M. Lehmann, S. Malik, D. Wu, J. L. Font, J. M. Bidlack, and A. V. Smrcka. 2006. Differential targeting of $G\beta\gamma$-subunit signaling with small molecules. *Science.* 312:443–446.
34. Semplicini, A., L. Lenzini, M. Sartori, I. Papparella, L. A. Calo, E. Pagnin, G. Strapazzon, C. Benna, R. Costa, A. Avogaro, G. Ceolotto, and A. C. Pessina. 2006. Reduced expression of regulator of G-protein signaling 2 (RGS2) in hypertensive patients increases calcium mobilization and ERK1/2 phosphorylation induced by angiotensin II. *J. Hypertens.* 24:1115–1124.
35. Hata, J. A., M. L. Williams, J. N. Schroder, B. Lima, J. R. Keys, B. C. Blaxall, J. A. Petrofski, A. Jakoi, C. A. Milano, and W. J. Koch. 2006. Lymphocyte levels of GRK2 (betaARK1) mirror changes in the LVAD-supported failing human heart: lower GRK2 associated with improved beta-adrenergic signaling after mechanical unloading. *J. Card. Fail.* 12: 360–368.
36. Ruiz de Azua, I., E. Del Olmo, A. Pazos, and J. Salles. 2006. Transmembrane signaling through phospholipase C-beta in the developing human prefrontal cortex. *J. Neurosci. Res.* 84:13–26.
37. Lanzara, R. 2005. Optimal agonist/antagonist combinations maintain receptor response by preventing rapid beta-1 adrenergic receptor desensitization. *Intl. J. Pharmacol.* 1:122–131.
38. Nestler, E. J. 2005. Is there a common molecular pathway for addiction? *Nat. Neurosci.* 8:1445–1449.
39. Lee, S., B. Howell, and P. Kunapuli. 2006. Cell imaging assays for g protein-coupled receptor internalization: application to high-throughput screening. *Methods Enzymol.* 414:79–98.
40. Conway, B. R., L. K. Minor, J. Z. Xu, J. W. Gunnet, R. DeBiasio, M. R. D'Andrea, R. Rubin, R. DeBiasio, K. Giuliano, L. DeBiasio, and K. T. Demarest. 1999. Quantification of G-protein coupled receptor internatilization using G-protein coupled receptor-green fluorescent protein conjugates with the ArrayScantrade mark high-content screening system. *J. Biomol. Screen.* 4:75–86.
41. Haasen, D., A. Schnapp, M. J. Valler, and R. Heilker. 2006. G protein-coupled receptor internalization assays in the high-content screening format. *Methods Enzymol.* 414:121–139.